PHYSICAL REVIEW E **90**, 010302(R) (2014)

Effective attenuation length of an electron in liquid water between 10 and 600 eV

Yoshi-Ichi Suzuki,[1] Kiyoshi Nishizawa,[2] Naoya Kurahashi,[1] and Toshinori Suzuki[1,2,*]

[1]*Department of Chemistry, Graduate School of Science, Kyoto University, Kitashirakawa-Oiwakecho, Sakyo-Ku, Kyoto 606-8502, Japan*

[2]*RIKEN Center for Advanced Photonics, RIKEN, Wako 351-0198, Japan*

(Received 23 December 2013; revised manuscript received 19 February 2014; published 14 July 2014)

The absolute values of the effective attenuation length of an electron in liquid water are determined using soft x-ray O1*s* photoemission spectroscopy of a liquid beam of water without employing any theoretical estimation or computationally obtained value. The effective attenuation length is greater than 1 nm in the entire electron kinetic energy region and exhibits very flat energy dependence in the 10–100 eV region.

DOI: 10.1103/PhysRevE.90.010302 PACS number(s): 78.70.−g, 79.60.−i, 82.80.Pv

When a high-energy particle or photon strikes a living cell, photoelectrons are ejected from cell water and they induce various chemical reactions and energy transfer processes. These scattering dynamics of electrons in liquid water are not only fundamental in condensed matter physics but also crucial for understanding radiation chemistry and biology. Electron scattering in water at high electron kinetic energies (>200 eV) is primarily electronic inelastic scattering, inducing ionization and electronic excitation (and dissociation) of water molecules [1–3]. The integral cross sections of electronic inelastic scattering and inelastic mean free path (IMFP) are estimated using the Bethe surface constructed from inelastic x-ray scattering data of liquid water [4]. The IMFP thus calculated commonly exhibit a so-called "universal curve" with the minimum in the electron kinetic energy (eKE) region between 50 and 100 eV and a rapid increase in the low- and high-energy sides. However, the absolute values estimated using different theoretical methods are significantly scattered as seen in Fig. 1(a). Experimental IMFP is not available for liquid water and only reported for amorphous ice [5], shown as circles (IMFP4) in Fig. 1(a). Theoretical estimates (IMFP1–3, shown in lines) for liquid water differ from these data points for amorphous ice [6,7].

Electron scattering at low kinetic energies (<100 eV) is particularly important for radiation chemistry, in which the IMFP is insufficient for describing electron transport and scattering. This is because elastic and vibrational inelastic scattering become increasingly important at low energies. When an electron undergoes multiple (pseudo)elastic scattering events prior to electronic inelastic scattering, the distance between the two electronic inelastic scattering events becomes shorter than the IMFP [Fig. 1(b)]. The distance at which the flux of electrons maintaining the initial kinetic energy diminishes by a factor of $1/e$ is termed the effective attenuation length (EAL), which is practically more important than the IMFP and also considerably easier to evaluate experimentally. The EAL is never larger than the IMFP at low energies and the two eventually coincide at high energies, because elastic and vibrational inelastic scattering become unimportant at higher energies. Thus, the EAL provides the lower bound for the IMFP. Previously, Ottosson *et al.* estimated the relative values of the EAL using O1*s* photoemission intensity of liquid water [8]. However, they incorrectly assumed energy-independent photoemission anisotropy, so that Thürmer *et al.* refined the analysis [9]. The relative EAL thus estimated exhibits a monotonous increase with the eKE in the region of 25–1000 eV. However, the absolute value of the EAL was not determined and the overall scale was adjusted to explain the photoemission intensities of electrolytes in solution using the computed depth profiles of the solute density.

In this study, we experimentally estimate the absolute values of the EAL in liquid water for the eKE range of 10–600 eV. To this end, we only employ experimental values such as the O1*s* photoemission spectra of liquid water and the integral and differential photoionization cross sections of liquid and gaseous water [9–11]. We illuminate a beam of liquid water in vacuum with soft x-ray radiation and measure photoemission both from the liquid water and evaporated gas [Fig. 1(c)]. The signal from the liquid is proportional to the number density of water molecules within the depth equal to the EAL (or more rigorously the mean escape depth), while the photoemission signal from the gas is proportional to the number density decreasing inversely proportional to the distance from the liquid surface. The gas density just above the liquid can be assumed to be a saturated vapor pressure of water at a given temperature. From these considerations, the absolute value of the EAL can be determined without employing any theoretical estimate or computationally obtained value.

The fundamental design of our photoelectron spectrometer has been described elsewhere [12]. The electron energy analyzer is a hemispherical electrostatic analyzer (Gammadata-Scienta SES100) with an ultimate resolution of 6 meV. We obtained most of the experimental results in the a-branch of BL17SU at the synchrotron radiation facility SPring-8, while we repeated measurements for the electron kinetic energies less than 40 eV at the b-branch of BL17SU. Between these two experiments, the focusing and polarization of the soft x-ray beams were different, and the photoelectron spectrometer was also modified. Despite such differences, the two sets of EAL data were in agreement for the overlapping energy region.

The liquid discharging nozzle is a straight fused silica capillary of 25 μm inner diameter and 7 mm length. A high-performance liquid chromatography pump is employed to transport sample solutions. Two metal-sintered filters with pore diameters of 2 and 0.5 μm are installed between the high-performance liquid chromatography pump and the nozzle. The nozzle assembly is mounted on an XYZ manipulator for fine positioning of the nozzle relative to the excitation light and the analyzer. At the photoionization point 1 mm downstream

*suzuki@kuchem.kyoto-u.ac.jp

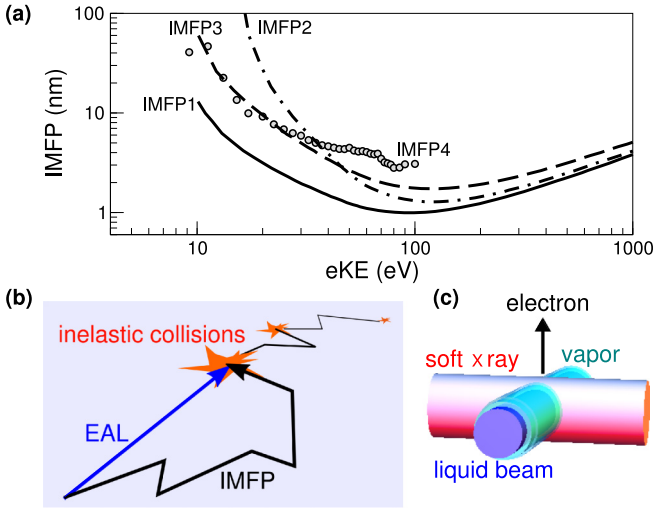

FIG. 1. (Color online) (a) Inelastic mean free path (IMFP) of electron in water. IMFPs are calculated using Mermin's model (IMFP1) and the Ashley model (IMFP2) [6] and a simplified KO model with the *e-e* dielectric function (IMFP3) [6,7]. IMFP4 shown as circles is obtained from the electronic inelastic scattering cross section in amorphous ice [5]. (b) Illustration of IMFP and EAL of an energetic electron. (c) Schematic view of the liquid beam x-ray photoelectron spectroscopy. See Fig. 3 for more details of the experimental geometry.

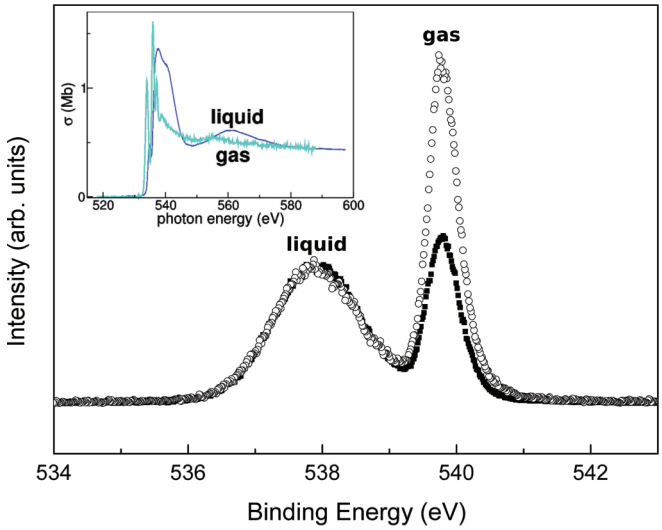

FIG. 2. (Color online) O1*s* photoelectron spectra of 0.14 M aqueous NaCl solution observed with 911 eV photon (open circle) and 1140 eV photon (filled square). The inset shows the photoabsorption cross sections for liquid [11] and gaseous [10] water. The cross section of liquid water is normalized for that of the gas in the region over 580 eV. These spectra were measured in the a-branch of BL17SU soft x-ray beamline of SPring-8.

from the nozzle, the liquid temperature of the water beam is estimated to be around 280 K [13]. The Reynolds number R_e of our liquid beam, defined as $R_e = 2v r\rho/\eta$, is 560 at a typical flow rate of 0.6 ml/min, where v is the velocity of the fluid (20 m/s), r is the radius of the capillary, ρ is the fluid density, and η is the fluid viscosity. It is generally accepted that if the Reynolds number is below 2000, the flow is laminar. The liquid beam breaks up into droplets at around 3 mm downstream from the nozzle. The propagation directions of the liquid beam and photon beam, and the electron detection axis are orthogonal to each other.

The soft x-ray radiation illuminates the liquid beam and evaporated gases around the liquid beam simultaneously, so that the O1*s* spectrum exhibits the liquid and vapor contributions. Figure 2 shows the O1*s* photoelectron spectra of the aqueous 0.14 M NaCl solution at 1140 and 911 eV excitation energies. Two bands at binding energies (BEs) of 539.79 and 537.96 eV in the spectra are assigned to the vapor and liquid contributions, respectively. The vapor contribution (BE = 539.79 eV) is utilized for energy calibration of the spectra [14]. Liquid contributions centered at 537.96 eV are much broader than the gas contributions; the FWHM of the vapor and liquid contributions are, respectively, 0.59 and 1.54 eV in the spectrum obtained at a photon energy of 1140 eV. Similar widths were observed at 911 eV. The gas to liquid energy shift is 1.8 eV, which is in reasonable agreement with the more accurate value of 1.6 eV recently redetermined [15]. Owing to the large spot size of soft x-ray radiation in our experiment using the direct beam in the a-branch, photoemission of evaporated molecules is emphasized in the spectra. The measured spot size is presented in Figs. S1 and S2 in the Supplemental Material [16]. The horizontal length of the photon beam is almost constant, while the vertical length varies with the photon energy. The photoabsorption cross section in the photon energy (ϵ) range of 540–1140 eV is 0.085–0.8 Mb [10]. Even if we assume the cross section to be the largest possible value of 1 Mb, the penetration depth of soft x-ray radiation into water is 330 nm, which is considerably larger than the EAL. Therefore, attenuation of the x-ray beam along the path from the liquid surface, on the illumination side, can be safely neglected in the following discussion.

Water vapor is isotropically distributed around the liquid beam. At high electron kinetic energy, where EAL is equal to the IMFP, only the electrons with an initial velocity oriented toward the detector are observed. Thus, the photoemission signal originates from the blue-colored area ($= r_0 \times$EAL) in Fig. 3(a). On the other hand, at low electron kinetic energy, elastic scattering occurs with an isotropic angular distribution. Then, the observed signal originates from the orange-colored area in Fig. 3(b). Using a geometrical factor $\pi/2$ [17], the EAL is obtained from the following relation to the area $a(E)$:

$$a(E) = \frac{\pi}{2} r_0 \times \mathrm{EAL}, \tag{1}$$

where $E(= \epsilon - \mathrm{BE})$ is the eKE and r_0 is the radius of a liquid beam. Since our main interest is the EAL at low energies (<100 eV), we employ Eq. (1) in the following discussion. This, however, leads to underestimation of the EAL at higher energies. Its correction is discussed later.

The photoelectron intensity from gas molecules at a given photon energy is expressed by the following equation:

$$I_g(E) = c_g(E) n_g(\epsilon) \sigma_g(\epsilon) f(\epsilon), \tag{2}$$

where $c_g(E)$ is a sensitivity factor, $n_g(\epsilon)$ is the number of ionized molecules in the detectable region, $\sigma_g(\epsilon)$ is the photoionization cross section, and $f(\epsilon)$ is the flux of photons.

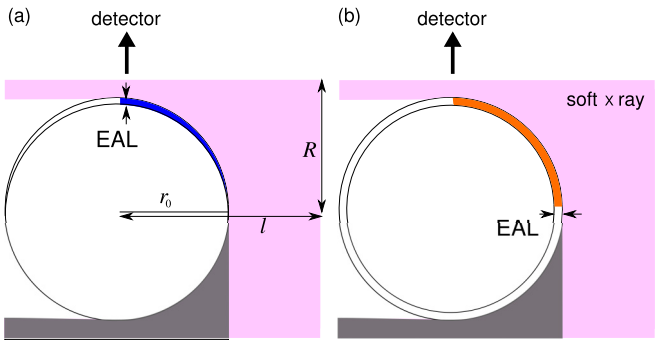

FIG. 3. (Color online) The cut view of the liquid beam in the plane defined by the x-ray propagation direction and the electron detection axis. Illustration of the effective ionization area of vapor and liquid beams for (a) few and (b) many elastic scattering events. r_0 and R are the radius of the liquid beam and x ray, respectively, while l represents the visible area for the detector. The gray area indicates the opposite side of the detector.

The photoelectron intensity from the liquid is similarly expressed as follows:

$$I_l(E) = c_l(E)\rho_l a(E)\sigma_l(\epsilon)f(\epsilon), \tag{3}$$

where $c_l(E)$ is a sensitivity factor, ρ_l is the density of molecules, and $\sigma_l(\epsilon)$ is the photoionization cross section.

The soft x-ray absorption spectra of gaseous [10] and liquid [11,18] water are quite similar in the region higher than 580 eV owing to their atomic nature: $\sigma_g(\epsilon) = \sigma_l(\epsilon)$. On the other hand, $\sigma_l(\epsilon)$ is larger than $\sigma_g(\epsilon)$ in the region less than 546 eV and around 560 eV [10,11], shown as the inset in Fig. 2. These differences were explicitly considered in our analysis.

The density of gas molecules diminishes with the distance r from the liquid beam in the long range. The $1/r$ dependence of gas density in the long distance was experimentally confirmed as presented in the Supplemental Material (Fig. S4) [16]. Then, the total number of molecules in the gas phase up to the radius R is approximated as

$$n_g(\epsilon) = \rho_g(T)\int_{-l}^{l}\int_{-R(\epsilon)}^{R(\epsilon)}\frac{r_0}{\sqrt{x^2+y^2}}dx'dy', \tag{4}$$

where l is the length of the photoionization region along the photon beam observed by the electron spectrometer (Fig. S3). The primes of $dx'dy'$ indicate that the region of integration excludes the backside of the x-ray radiation and the detector. $R(E)$ is one-half of the spot size of x-ray radiation (vertical length, Fig. S1) [16]. $\rho_g(T)$ is the saturated vapor density of H_2O at temperature T [19]. The uncertainty in temperature is expected to be ± 5 K, resulting in -28% (-5 K) and $+38\%$ ($+5$ K) in $\rho_g(T)$.

The sensitivity factors $c_l(E)$ and $c_g(E)$ are influenced by photoelectron angular anisotropy, since the photoelectrons are observed with a finite detection solid angle. The photoelectron angular distribution can be expressed as [20]

$$\frac{d\sigma(E)}{d\Omega} = \frac{\sigma(E)}{4\pi}\left\{1+\frac{\beta(E)}{4}[3P\cos(2\theta)+1]\right\}, \tag{5}$$

where $\sigma(E)$ is the integral photoionization cross section, $\beta(E)$ is the photoemission anisotropy parameter, and θ is the angle between the photoelectron velocity vector and the linear polarization of the photon beam. The polarization degree P is defined as follows:

$$P = \frac{I_x - I_y}{I_x + I_y}, \tag{6}$$

where I_x is the intensity along the electron detection axis and I_y is the intensity perpendicular to that axis. The degree of polarization also varies with the photon energy. We employed the β values reported for gaseous and liquid water [9] and calculated the sensitivity factor for a given photoelectron kinetic energy. The influence of different β values between liquid and gas is 10%–50% in the energy range of 10–500 eV (Table S1 [16]).

Considering these factors, the intensity ratio between the gas and liquid photoelectron signals is given by

$$\frac{I_l(E)}{I_g(E)} = \frac{c_l(E)}{c_g(E)}\frac{\sigma_l(\epsilon)}{\sigma_g(\epsilon)}\frac{\rho_l a(E)}{n_g(\epsilon)} \tag{7}$$

$$\equiv A(E)\mathrm{EAL}, \tag{8}$$

where $A(E)$ is the energy dependent instrumental correction factor. From this equation, one obtains

$$\mathrm{EAL} = \frac{1}{A(E)}\frac{I_l(E)}{I_g(E)}. \tag{9}$$

The O1s band appears on a continuous background of secondary electrons originating from valence photoemission, so that we evaluated the O1s intensity by subtracting the background. This procedure, however, becomes less accurate for the lowest eKE region less than 10 eV owing to instability of the background.

The EAL values extracted using Eq. (1) are shown in Fig. 4 as the filled blue triangles. The liquid temperature was assumed to be 280 K and the photoemission anisotropy [9] was taken into account. The light blue triangles are the values scaled as the factor $\pi/2$, presenting the upper bound of EAL. The actual EAL values should be closer to the blue triangles at low energies and closer to the light-blue triangles at high energies. Although we do not know how the EAL varies between these two boundaries, we present a guide for the eyes as a green line as a plausible EAL curve, as shown in Fig. 4. The solid line (IMFP1) is the IMFP estimated using the Bethe surface. This particular IMFP was calculated using Mermin's modeling of the Bethe surface; however, since the theoretical surface is compatible with the experimental one [6], this estimate of IMFP is essentially based on experimental measurements. It is only noted that the absolute value of the experimental Bethe surface is normalized using the Thomas-Reiche-Kuhn sum rule. Our EAL values are larger than IMFP1 in the energy region higher than 20 eV. Since the EAL provides a lower bound for the IMFP, these results are in disagreement by a factor of 2 to 3 in the eKE region higher than 100 eV.

It is worth examining possible sources of errors that make our EAL apparently larger than the real values. If evaporated gas stagnates in expanding from the liquid surface into vacuum, the actual density of water vapor becomes higher than our estimate. In this case, our EAL becomes even greater than shown in Fig. 4, so that this is not regarded as a problem. Another possibility is scattering in vapor. Since the

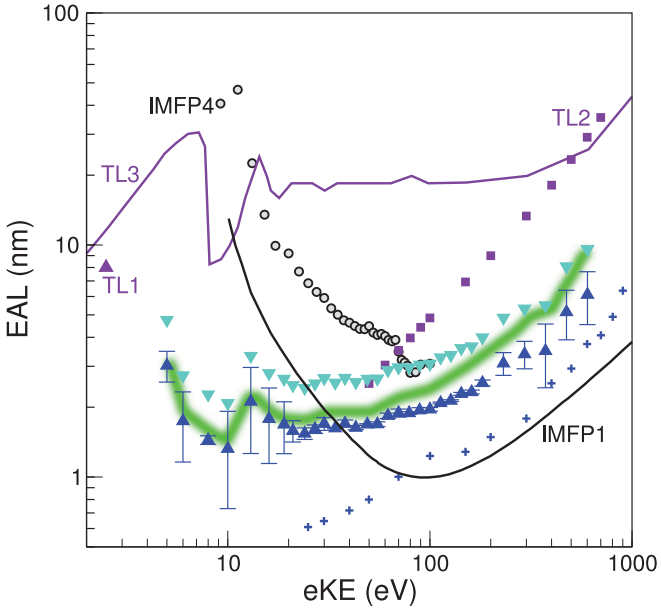

FIG. 4. (Color online) Effective attenuation length (EAL) as a function of electron kinetic energy (eKE) (also in Table S1 [16]), and thermalization length (TL) and inelastic mean free path (IMFP). The error bars result from data sets on different days. The filled triangles (blue) and filled-inverted triangles (light blue) indicate the EAL, assuming 280 K, with and without the $\pi/2$ geometrical factor. The thick green line is a guide for the eyes as a possible EAL curve affected by the $\pi/2$ factor at high energies. The EAL values reported by Thürmer *et al.* are indicated by the plus signs. Experimental TL is obtained from the photocurrent in solutions (TL1) [21]. TL2 is the continuous slowing down approximation range [22], and TL3 is the penetration length of an electron [23] in water. The IMFP1 (line) and IMFP4 (circles) are the same as in Fig. 1.

photoelectrons emitted from the liquid surface travel a longer distance through a dense water vapor than those emitted from the vapor, the liquid signal is relatively underestimated. The underestimation, however, is only by 13% at a 24 μm distance (typical x-ray spot size) from liquid surface, assuming the $1/r$ distribution of vapor and the Lambert-Beer law with the largest value of the inelastic cross section (~400 Mb at the eKE of 100 eV [24]). Hence, the effect on EAL is at most 13%. The third one is the liquid temperature, which we estimated based on a previous study using Raman thermometry [13]. If our estimate of the temperature is too low, the real EAL will be greater than shown in Fig. 4. Thus, the only possibility that our EAL becomes closer to IMFP1 at higher energies is the case that the actual liquid temperature is lower than 280 K. However, even if we assume the liquid temperature to be 275 K, the EAL decreases only by 28% and the plausible EAL curve is still larger than IMFP1 in the energy region higher than 100 eV.

The thermalization length (TL) of an electron, the distance between the creation point of an electron and the final point where the electron is thermalized, is particularly relevant to radiation chemistry. The TL is always larger than the EAL. As seen in Fig. 4, Watt's TL, or the continuous slowing down approximation range [22], appears to be close to our EAL at around 50 eV, which suggests that Watt's TL is too short at that energy. Our EAL is more consistent with a longer TL (TL3 in Fig. 4) by Uehara and Nikjoo [23]. It is noted, however, that the comparison is qualitative, because the theoretical estimates of TL also contain a number of assumptions. For example, vibrational inelastic scattering is simply neglected or its cross section is substituted by the value in amorphous ice.

Our result clearly indicates that the observed EAL is very flat over the region of 10–100 eV. This is an important result in elucidation of electron scattering dynamics in liquid water in relation to radiation chemistry and biology. The results also imply that the probing depth of photoelectron spectroscopy is not strongly dependent on electron kinetic energy in this range, which is valuable information for photoemission spectroscopy of liquids using UV light sources such as synchrotron radiation, laser high harmonics generation, and free electron lasers.

We would like to thank Dr. Masaki Oura for providing us with the soft x-ray polarization and spot size data. We thank Shutaro Karashima for his experimental assistance. The synchrotron radiation experiments were performed at BL17SU of SPring-8 with the approval of RIKEN (Proposal No. 20130075).

[1] H. Nikjoo, S. Uehara, and D. Emfietzoglou, *Interaction of Radiation with Matter* (CRC Press, Boca Raton, FL, 2012).
[2] M. Dingfelder, R. H. Ritchie, J. E. Turner, W. Friedland, H. G. Paretzke, and R. N. Hamm, Radiat. Res. **169**, 584 (2008).
[3] I. Plante and F. A. Cucinotta, New J. Phys. **11**, 063047 (2009).
[4] H. Hayashi, N. Watanabe, Y. Udagawa, and C.-C. Kao, Proc. Natl. Acad. Sci. USA **97**, 6264 (2000).
[5] M. Michaud, A. Wen, and L. Sanche, Radiat. Res. **159**, 3 (2003).
[6] D. Emfietzoglou, I. Kyriakou, I. Abril, R. Garcia-Molina, and H. Nikjoo, Int. J. Radiat. Biol. **88**, 22 (2012).
[7] D. Emfietzoglou, I. Kyriakou, R. Garcia-Molina, I. Abril, and H. Nikjoo, Radiat. Res. **180**, 499 (2013).
[8] N. Ottosson, M. Faubel, S. E. Bradforth, P. Jungwirth, and B. Winter, J. Electron Spectrosc. Relat. Phenom. **177**, 60 (2010).
[9] S. Thürmer, R. Seidel, M. Faubel, W. Eberhardt, J. C. Hemminger, S. E. Bradforth, and B. Winter, Phys. Rev. Lett. **111**, 173005 (2013).
[10] J. Berkowitz, *Atomic and Molecular Photoabsorption: Absolute Total Cross Sections* (Academic, New York, 2002).
[11] S. Schreck, G. Gavrila, C. Weniger, and P. Wernet, Rev. Sci. Instrum. **82**, 103101 (2011).
[12] K. Nishizawa, K. Ohshimo, and T. Suzuki, J. Chin. Chem. Soc. (Taipei) **60**, 1403 (2013).
[13] K. R. Wilson, B. S. Rude, J. Smith, C. Cappa, D. T. Co, R. D. Schaller, M. Larsson, T. Catalano, and R. J. Saykally, Rev. Sci. Instrum. **75**, 725 (2004).

[14] R. Sankari, M. Ehara, H. Nakatsuji, Y. Senba, K. Hosokawa, H. Yoshida, A. D. Fanis, Y. Tamenori, S. Aksela, and K. Ueda, Chem. Phys. Lett. **380**, 647 (2003).

[15] N. Kurahashi, S. Karashima, Y. Tang, T. Horio, B. Abulimiti, Y.-I. Suzuki, Y. Ogi, M. Oura, and T. Suzuki, J. Chem. Phys. **140**, 174506 (2014).

[16] See Supplemental Material at http://link.aps.org/supplemental/10.1103/PhysRevE.90.010302 for figures of parameters of the soft x-ray radiation and a table of the observed effective attenuation length.

[17] B. Winter and M. Faubel, Chem. Rev. **106**, 1176 (2006).

[18] D. T. Bowron, M. H. Krisch, A. C. Barnes, J. L. Finney, A. Kaprolat, and M. Lorenzen, Phys. Rev. B **62**, R9223 (2000).

[19] W. Wagner and A. Pruss, J. Phys. Chem. Ref. Data **22**, 783 (1993).

[20] J. A. R. Samson and A. F. Starace, J. Phys. B: At. Mol. Phys. **8**, 1806 (1975).

[21] V. V. Konovalov, A. M. Raitsimring, and Y. D. Tsvetkov, Int. J. Radiat. Appl. Instrum. Part C **32**, 623 (1988).

[22] D. E. Watt, *Quantities for Dosimetry of Ionizing Radiations in Liquid Water* (Taylor & Francis, London, 1996).

[23] S. Uehara and H. Nikjoo, J. Radiat. Res. **47**, 69 (2006).

[24] Y. Itikawa and N. Mason, J. Phys. Chem. Ref. Data **34**, 1 (2005).